January 2013

Cerium oxide nanoparticles: influence of the high-Z component revealed on radioresistant 9L cell survival under X-ray irradiation

Adam Briggs
University of Wollongong, arb938@uowmail.edu.au

stephanie corde
University of Wollongong, scorde@uow.edu.au

Sianne Oktaria
University of Wollongong, so819@uowmail.edu.au

Ryan Brown
University of Wollongong, rsb084@uowmail.edu.au

Anatoly B. Rosenfeld
University of Wollongong, anatoly@uow.edu.au

See next page for additional authors

Cerium oxide nanoparticles: influence of the high-Z component revealed on radioresistant 9L cell survival under X-ray irradiation

Abstract

This article pioneers a study into the influence of the high-Z component of nanoparticles on the efficacy of radioprotection some nanoparticles offer to exposed cells irradiated with X-rays. We reveal a significant decrease in the radioprotection efficacy for cells exposed to CeO2 nanoparticles and irradiated with 10 MV and 150 kVp X-rays. In addition, analysis of the 150 kVp survival curve data indicates a change in radiation quality, becoming more lethal for irradiated cells exposed to CeO2 nanoparticles. We attribute the change in efficacy to an increase in high linear energy transfer Auger electron production at 150 kVp which counterbalances the CeO2 nanoparticle radioprotection capability and locally changes the radiation quality. This study highlights an interesting phenomenon that must be considered if radiation protection drugs for use in radiotherapy are developed based on CeO2 nanoparticles.

Keywords

radioresistant, 9l, cell, survival, under, x, ray, irradiation, nanoparticles, influence, high, z, component, cerium, revealed, oxide

Disciplines

Medicine and Health Sciences

Publication Details

Briggs, A., corde, s., Oktaria, S., Brown, R., Rozenfeld, A., Lerch, M., Konstantinov, K. & Tehei, M. (2013). Cerium oxide nanoparticles: influence of the high-Z component revealed on radioresistant 9L cell survival under X-ray irradiation. Nanomedicine, 9 (7), 1098-1105.

Authors

Adam Briggs, stephanie corde, Sianne Oktaria, Ryan Brown, Anatoly B. Rosenfeld, Michael Lerch, Konstantin Konstantinov, and Moeava Tehei

Title: Cerium oxide nanoparticles: Influence of the high-Z component revealed on radioresistant 9L cell survival under X-ray irradiation

Article Type: Original Article

Keywords: Cerium oxide nanoparticles; High-Z; Radioprotectors; Photoelectric effect; Radioresistant.

Corresponding Author: Dr. Moeava Tehei, Ph D.

Corresponding Author's Institution: UOW

First Author: Adam Briggs

Order of Authors: Adam Briggs; Stéphanie Corde; Sianne Oktaria; Ryan Brown; Anatoly Rosenfeld; Michael Lerch; Konstantin Konstantinov; Moeava Tehei, Ph D.; Moeava Tehei

Abstract: This article pioneers a study into the influence of the high-Z component of nanoparticles on the efficacy of radioprotection some nanoparticles offer to exposed cells irradiated with X-rays. We reveal a significant decrease in the radioprotection efficacy for cells exposed to CeO2 nanoparticles and irradiated with 10 MV and 150 kVp X-rays. In addition, analysis of the 150 kVp survival curve data indicates a change in radiation quality, becoming more lethal for irradiated cells exposed to CeO2 nanoparticles. We attribute the change in efficacy to an increase in high linear energy transfer Auger electron production at 150 kVp which counterbalances the CeO2 nanoparticle radioprotection capability and locally changes the radiation quality. This study highlights an interesting phenomenon that must be considered if radiation protection drugs for use in radiotherapy are developed based on CeO2 nanoparticles.

***Graphical Abstract: Text**

A counterbalance exists between radioprotection and enhancement for CeO_2 NPs. The influence of this high-Z property is revealed on radioresistant 9L cells, where greater radioprotection was achieved using 10 MV photons in comparison to that achieved when using 150 kVp X-rays. At lower energies, high-LET Auger electron cascades create clustered, indirect and dominant direct damages and free radicals that are scavenged by CeO_2 or recombine resulting in formation of H_2O. Conversely, at higher energies, low-LET secondary electrons create dominantly free radicals that both: are scavenged by CeO_2 NPs and can indirectly damage DNA. This unique mechanism should be considered throughout all nanoparticle based radiotherapy where high-Z nanoparticles such as CeO_2 are used.

*Graphical Abstract: Image

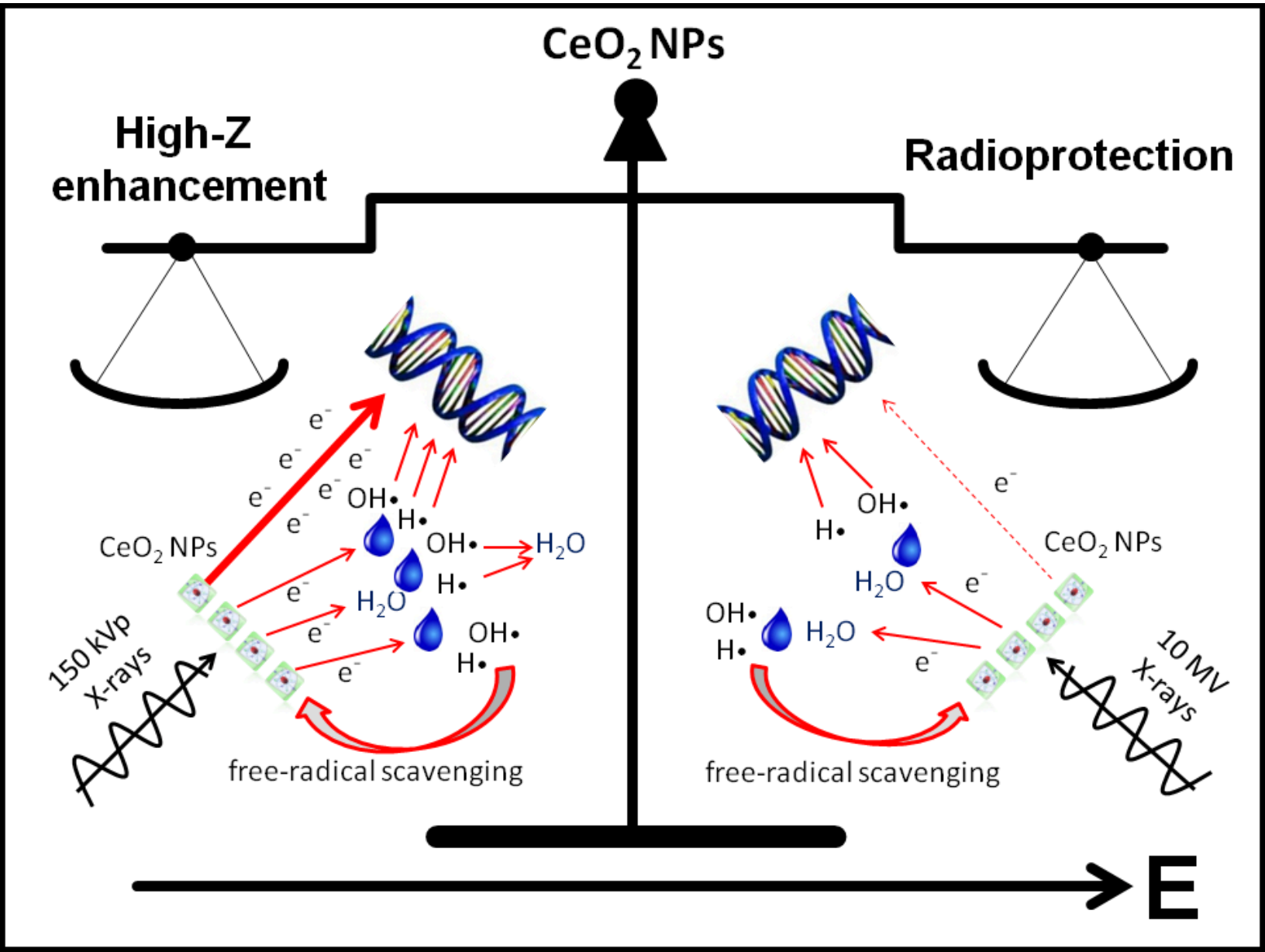

Cerium oxide nanoparticles: Influence of the high-Z component revealed on radioresistant 9L cell survival under X-ray irradiation

Adam Briggs, BMedRadPhysAdv[a,b], Stéphanie Corde, PhD[a,c], Sianne Oktaria, MMedRadPhys[a,b,d], Ryan Brown, BMedRadPhysAdv[a,b], Anatoly Rosenfeld, PhD[a,b], Michael Lerch, PhD[a,b], Konstantin Konstantinov, PhD[f,b], Moeava Tehei, PhD[d,b,e,*]

[a] *Centre for Medical and Radiation Physics, University of Wollongong, NSW, Australia*
[b] *Illawarra Health and Medical Research Institute, University of Wollongong, NSW, Australia*
[c] *Radiation Oncology Department, Prince of Wales Hospital, Randwick, NSW, Australia*
[d] *Centre for Medical Bioscience, University of Wollongong, NSW, Australia*
[e] *School of Chemistry, University of Wollongong, Wollongong, NSW, Australia*
[f] *Institute for Superconducting and Electronic Materials, University of Wollongong, NSW, Australia*

Short title: Effect of high-Z components revealed on CeO_2 NPs (48 characters inc. spaces)

Sources of research support: AINSE research fellowship, small UoW Near Miss grant and a small URC grant

Abstract word count: 135

Manuscript word count: 4920

Number of figures: 4

Number of tables: 1

Number of references: 38

*Corresponding author. Centre for Medical Bioscience, University of Wollongong, Northfields Avenue, Wollongong, NSW 2522, Australia.
Email address: moeava@uow.edu.au (Moeava Tehei, PhD)

Abstract

This article pioneers a study into the influence of the high-Z component of nanoparticles on the efficacy of radioprotection some nanoparticles offer to exposed cells irradiated with X-rays. We reveal a significant decrease in the radioprotection efficacy for cells exposed to CeO_2 nanoparticles and irradiated with 10 MV and 150 kVp X-rays. In addition, analysis of the 150 kVp survival curve data indicates a change in radiation quality, becoming more lethal for irradiated cells exposed to CeO_2 nanoparticles. We attribute the change in efficacy to an increase in high linear energy transfer Auger electron production at 150 kVp which counterbalances the CeO_2 nanoparticle radioprotection capability and locally changes the radiation quality. This study highlights an interesting phenomenon that must be considered if radiation protection drugs for use in radiotherapy are developed based on CeO_2 nanoparticles.

Keywords: Cerium oxide nanoparticles, High-Z, Radioprotectors, Photoelectric effect, Radioresistant

The application of nanotechnology to medicine provides an innovative approach that can enhance the effectiveness of radiotherapy[1]. Targeted and non-targeted tissues and cells are, in general, damaged along an indirect pathway during radiation treatment as a result of the production of free radicals[2]. Free radical production can result in chemical reactions that damage DNA molecules and initiates apopotosis and mitotic death[3,4]. The protective mechanisms of a cell in response to ionizing radiation exposure are insufficient and have prompted the research and development of novel nanoparticles (NPs) with the ability to enhance or assist cell protective mechanisms. If such NPs act preferentially and protect normal tissues that surround target tissues it would allow dose escalation to the target for better tumour control and hence improved patient outcomes.

One novel nanoparticle currently under investigation for its ability to provide protection against

radiation induced damage is cerium oxide (CeO_2)[5]. Previous studies investigated the free-radical scavenging effectiveness of CeO_2 NPs to provide radioprotection *in vitro* for a variety of normal cell lines, and *in vivo* with athymic nude mice[6,7]. CeO_2 NPs inherit an autoregenerative cycle (Ce^{3+}– Ce^{4+}– Ce^{3+}) that enables continued antioxidant activity, providing long-term scavenging of reactive oxygen species (ROS)[8]. CeO_2 NPs now offer a prospective alternative to the only clinically used radioprotector — amifostine[9]. Amifostine has the limitation of considerable side effects, a short half-life in serum and high cost caused by frequent dosing requirements[3].

Many avenues need to be explored prior to the clinical acceptance of CeO_2 NPs and its application as a radioprotector. Current investigations using CeO_2 NPs explore characteristics such as: its bioavailability/toxicity[10–12], the ability to provide radiation protection by scavenging free radicals and the selective nature of its protection to normal and cancerous cells[7]. However, steps towards the clinical acceptance of CeO_2 NPs requires an understanding of its effectiveness across a range of beam energies. To the best of our knowledge, the influence of the above effects have never been reported in the literature.

X-rays used throughout clinical treatments produce free radicals through interactions with matter[2]. Interactions of interest include — photoelectric and Compton effects, coherent scattering along with pair production at higher energies. The most influential factors dictating the cross-section for these interactions is the radiation energy (E) and atomic number (Z). The mass attenuation coefficient due to the photoelectric effect is approximately proportional to $(Z/E)^3$, where Z is the atomic number of the absorbing medium and E is the photon energy[13]. The use of high-Z nanoparticles (i.e. gold NPs, $Z_{Au} = 79$) in dose enhancement provides an example of how we can exploit the dependence of the photoelectric effect[13–15]. The majority of Auger electrons are produced as a consequence of the photoelectric effect supporting the notion that their greatest abundance is achieved when the cross-section for the photoelectric effect is maximised. Compton interactions occur with outer shell electrons and subsequently, have no significant Z dependence[16]. A threshold photon energy of 1.022 MeV exists for pair production, with a cross section that increases rapidly with energy above the threshold[13]. Furthermore, pair production cross-section has a quadratic proportionality with Z. The linear energy transfer (LET) is a measure of the energy locally imparted to a medium by a secondary charged particle of energy (E) along its path[2,16]. The variation of the LET with decreasing electron energy is an important

consideration in our study as increases in LET correspond to increases in the relative biological effectiveness (RBE) of the radiation field[17]. Auger electrons have a LET that lies in the range of 10 - 25 keV/μm[18] while the positron-electron pair produced during the pair production process with kinetic energy of a few MeV have a LET of 0.2 keV/μm[17]. Ultimately, Auger electrons deposit their energy along their tracks in a very short range, indicating an increase in the biological effectiveness of radiation exposure at lower energies[13]. CeO_2 is a known radioprotector however, the high-Z ($Z_{Ce} = 58$) component of this material is the major contributor towards potential increases in the RBE.

In this article, we postulate that CeO_2 NPs efficacy to function as a radioprotector is dependent on the energy of X-rays used during treatment and we investigated this energy-dependence using 150 kVp X-ray and 10 MV photon beams. Furthermore, to prove the existence of any high-Z enhancement abilities that CeO_2 may possess, we select the radioresistant 9L cell line.

Cell survival curves are an effective analytical method that we utilise to measure the effectiveness of CeO_2 NPs to provide radioprotection. Radiobiological properties such as radiosensitivity and repair accumulation can be extracted using this analysis, where the influence on these parameters by the CeO_2 NP are determined for the first time.

Our study reveals an energy-dependent efficacy due to the influence of the high-Z component of CeO_2 NPs ($Z_{eff} = 54$). At 10 MV, indirect damage effects dominate and mainly results from the interaction of molecules contained in cells and the free radicals produced during the radiolysis of water. The radioprotection provided by CeO_2 NPs is achieved using free-radical scavenging effects, facilitating increased repair while lowering the cells radiosensitivity. At lower X-ray beam energies, the probability of direct damage effects become an increasingly important consideration and are no longer negligible[17]. Low energy secondary electrons have an increased probability to produce clusters of free radicals that can provoke the rupture of covalent bonds and scissions in the molecules contained within cells[17]. The additional presence of free radicals cannot be fully managed by the scavenging abilities of CeO_2, adding further weight to increased damaging effects at lower energies. The work described in this article reveals that the free-radical scavenging effect is counterbalanced by the high-Z atoms present in the elemental composition of CeO_2. These high-Z atoms are responsible for an increased production of lethally damaging, low energy secondary electrons.

Methods

Cell line

The rat brain gliosarcoma cell line (9L) was obtained from the European Collection of Cell Cultures (ECACC). Derived from a N-nitrosomethylurea-induced tumour, this adherent radioresistant cell line inherits glial morphology and has undergone routine mycoplasma contamination testing.

Cell culture

The 9L gliosarcoma cells were grown and maintained during their exponential growth phase in T75 cm^2 BD Falcon^{TM} tissue culture flasks (Franklin Lakes, NJ, USA) containing Dulbecco's Modified Eagle Medium (DMEM) with L-Glutamine, supplemented with 10% (v/v) Fetal Bovine Serum (FBS) and 1% (v/v) Penicillin/Streptomycin (PenStrep). Cell cultures were passaged upon reaching 85% confluence to a concentration of 2–4 $\times$ 10^4 cells/cm^2 and stored at 37°C in a 5% (v/v) CO_2 cell culture incubator. In our hands, the cell doubling time was deduced to be 36 h. All chemical reagents used were purchased from GIBCO®, unless indicated otherwise. All cell culture work was carried out at the Illawarra Health and Medical Research Institute (Wollongong, NSW, Australia).

Nanoparticle synthesis and preparation

The cerium oxide nanoparticle sample was synthesised at the Institute for Superconducting and Electronic Materials (Wollongong, NSW, Australia) using a spray pyrolysis technique[19,20]. This synthesis approach produces compounds of high purity and chemical homogeneity, yielding a nanoparticle with reproducible size and characteristics. A 1 L aqueous solution was prepared, consisting of 0.45 mol/L of $Ce(NO_3)_3$ and $6H_2O$. This solution was sprayed and decomposed at 500°C using a customised spray pyrolysis system designed for the engineering of nanoceramics and composites. Cerium oxide NP samples were dried prior to sterilisation using an open furnace operating at 140°C for a period no less than 2 h. Sterilisation was achieved using an autoclave operating at 121°C on a dry cycle, with sterilised samples kept in glass vials surrounded by silica gel to avoid moisture absorption. Cerium oxide NPs were dispersed in Dulbecco's Phosphate-Buffered Saline (DPBS) to solubilise the NP. Sonication and vortex mixing was used to minimise

the size of NP aggregates and increase the homogeneity of dispersion prior to exposure. A concentration of 50 μg/ml was applied to 9L cells for subsequent analysis.

X-ray Diffraction

A slurry of nanoparticle was produced via vigorous mixing with 100 % ethanol which was placed onto a quartz sample holder. The sample was presented to the monochromatic, copper Kα X-ray beam ($\lambda = 1.5406$ Å). The X-ray diffraction analysis was performed using an automated GBC® eMMA X-ray Diffractometer (GBC, VIC, Australia) where the sample was scanned using a step size of 0.2° 2θ through the range of 20° - 70° 2θ with a count time of 8.75 seconds per step. The operational settings used were 25 mA and 40 kVp. Phase identification was extracted by comparing the recorded diffraction pattern with the Inorganic Crystal Structure Database (ICSD). The average nanoparticle crystallite size ($\overline{Tc}$) is extracted from the X-ray diffraction data using Scherrer's equation (1).

$$\overline{Tc} = \frac{K\lambda}{\beta cos(\theta_B)} \tag{1}$$

K is the shape factor constant ($K = 0.89$), λ is the X-ray beam wavelength, β is the FWHM (in radians) and θ_B is the Bragg angle.

Transmission Electron Microscopy

Transmission electron microscopy (TEM) was performed using a JEOL 2011 high resolution (HR) instrument, characterising the size and morphology of the sample. The samples were prepared by dispersion of CeO_2 powders onto holey carbon support films.

Gas sorption analysis

The specific surface area of the powder samples was measured by the Brunauer-Emmett-Teller (BET) method with a Nova 1000 high speed gas sorption analyser from Quantachrome, using the adsorption of N_2 at the temperature of liquid nitrogen. Prior to measuring, the samples were degassed at 120°C for 2 h 30 min in vacuum.

Irradiation of cell culture

All irradiations were performed in the radiation oncology department at the Prince of Wales Hospital (Randwick, NSW, Australia). The confluent cell culture was irradiated following a 24 h incubation period with cerium oxide nanoparticles at a concentration of 50 μg/ml. Prior to megavoltage irradiation, non-vented T12.5 cm^2 tissue culture flasks (BD Falcon^{TM}) were completely filled with Hank's Balanced Salt Solution (HBSS) to ensure no air bubbles were present inside the flask, maximising the accuracy of the dose delivered at the depth of the cells. Kilovoltage irradiation was performed using only a 6 mm depth of medium in an attempt to maximise the accuracy of the dose delivered to the cell monolayer. Beam energies of 10 MV and 150 kVp were explored using an Elekta Axesse^{TM} LINAC (Elekta AB, Kungstensgatan, Stockholm, Sweden) and a Nucletron Oldelft Therapax DXT 300 Series 3 Orthovoltage unit (Nucletron B.V., Veenendaal, The Netherlands), respectively. All doses (1, 2, 3, 5 & 8 Gy) were delivered in single fractions at room temperature. Tissue culture flasks were irradiated in a horizontal orientation with solid water placed both underneath and around the sides of the flasks, primarily to maintain adequate backscattering effects and stabilise electronic equilibrium. Unirradiated control samples (with and without CeO_2 NPs) were utilised and handled under the same conditions as the irradiated samples.

Clonogenic cell survival assay

Cell survival was assessed using a clonogenic cell survival assay, otherwise known as a colony-forming assay[21,22]. Adherent cell lines, such as 9L, have the ability to form colonies *in vitro* even at low density cell seeding. Following radiation exposure, all of the flasks were promptly plated, initiating the clonogenic assay (duration of 15 doubling times for 9L cells). The growth media was removed and the confluent cell culture was thoroughly washed with DPBS containing no calcium (Ca) or magnesium (Mg) salts. The cells were then detached from the surface of the flask with a 2-3 minute incubation with 0.05% trypsin ethylenediaminetetraactic acid (Trypsin-EDTA), forming a cell suspension that was counted using a haemocytometer. Cells were seeded at low densities in triplicate into 100 mm Sigma-Aldrich® petri dishes containing 10 ml of the DMEM. All plates were incubated at 37°C and 5% CO_2 for 15 cell doubling times. Each prescribed dose used a maximum of three different cell seeding numbers, all determined by preliminary experiments to

narrow the optimal seeding to achieve an approximate number of colonies of 100. Following the incubation period, formed colonies were fixed and stained using a solution comprised of 75% (v/v) ethanol and 25% (v/v) crystal violet (Sigma-Aldrich®). Colonies containing 50 cells or more, confirmed by the use of a high powered inverted microscope are counted for analysis.
Cell survival data is presented using the relative surviving fraction of cells as a function of absorbed dose. The surviving fraction is extracted from the plating efficiency. The Plating Efficiency (PE) is calculated as the ratio of viable colonies to cells seeded.

$$PE = \frac{No.\ of\ colonies\ counted}{No.\ of\ cells\ seeded} \tag{2}$$

The Surviving Fraction (SF) was determined by comparing the PE at a given dose to the control (i.e. no dose). The surviving fraction is given by:

$$SF(D) = \frac{PE(D)}{PE(0)} \tag{3}$$

where SF(D) and PE(D) is the surviving fraction and plating efficiency at dose D (Gy), respectively.

PE(0) is the plating efficiency of unirradiated controls (0 Gy) with or without NPs used for normalisation of irradiated samples with or without NPs, respectively. The plating efficiencies given are the mean PE values from duplicate samples at each dose.

Statistical analysis

Cell survival experiments were replicated once and measured in triplicate on each occasion. The reported values are the mean of all experiments, with the experimental uncertainty given as one standard deviation. The LQ model was fitted to cell survival data using KaleidaGraph software. The fit of the data is weighted by the reported error at each dose in the determination of the radiobiological constants of the LQ model. Statistical analysis of toxicity data was performed using a two-tailed Student's t-test using the assumption of equal variance. A P value of ≤ 0.05 was considered statistically significant.

Cell survival analysis

The cell survival curves are constructed on a semi-logarithmic plot of the surviving fraction as a function of absorbed dose. The cell survival curve can be represented mathematically using the linear quadratic (LQ) model as X-ray (i.e. low LET) radiation sources are used[2,23].

$$SF(D) = exp(-\alpha D - \beta D^2) \tag{4}$$

The parameters α (Gy^{-1}) and β (Gy^{-2}) are measures of the radiosensitivity and repair accumulation, respectively. The surviving fraction data was fitted to the LQ model using KaleidaGraph software, extracting the α and β constants for each set of cell survival data.

Protection enhancement ratio

The Protection Enhancement Ratio (PER) is a value used to measure the degree of protection achieved using CeO_2 NPs. The PER can be defined as the ratio of doses in the presence of CeO_2 to the control (i.e. no NP), as measured at the common endpoint of 10 % cell survival.

$$PER_{SF=10\%} = \frac{Dose_{CeO_2}}{Dose_{control}} \tag{5}$$

A PER value greater than 1 is indicative of radioprotection, whereas a PER value less than 1 reveals a sensitisation effect. This effect is manifested as a direct result of the presence of CeO_2 NPs.

Results

Phase and structural characterisation of cerium oxide

The biochemical effect of nanoparticles are dependent on their structural and physical characteristics. Characteristics of particular interest include: phase composition, structure and crystallite size. First order diffraction peaks have been labelled (Figure 1, **A**) upon correlating recorded data against the ICSD (PDF card no. 01-089-8436). Cerium oxide nanoparticle's phase is confirmed to exist as CeO_2. This matches the phase of the cerium oxide NPs that have been reported to provide protection in response to exposure of ionising radiation[3,5–7]. Using the XRD

data, the structure of the sample can be extracted. The CeO_2 NP sample has a simple cubic crystalline structure with a single lattice parameter, a = 5.4112 Å. The average crystallite size can be extracted from the XRD peaks using Scherrer's equation. The most accurate analysis is achieved by selecting the most pronounced peaks, free of any contribution from surrounding satellite peaks. The average crystallite size was calculated to lie in the range of 6–8 nm, consistent with the crystallite sizes observed in the HR-TEM image (Figure 1, **B**). The high resolution transmission electron micrograph (HR-TEM) shows clear lattice fringes (Figure 1, **B**) with a fringe spacing (d) of 3.15 Å, which corresponds to the distance between the 111 lattice planes of CeO_2. The calculated BET specific surface area of the nanocrystalline powder was 51 m^2/g.

Toxicity of CeO_2 NPs to 9L cells

No definitive conclusions have been made regarding the toxicity of CeO_2 NPs[3,6,7,24]. Efforts to determine its biological viability remains the subject of numerous studies and is an integral component to the development of any model using CeO_2 [8,10,11,24–27]. Initially, we investigated the toxicity of our synthesised CeO_2 NP to 9L cells. The clonogenic cell survival assay was conducted following a 24 h incubation with CeO_2 NPs at a range of concentrations up to 500 μg/ml. We established that the application of CeO_2 NPs had no statistically significant toxic effect on the surviving fraction of 9L cells at 50 μg/ml (Figure 2) where we found a surviving fraction of 0.93 $\pm$ 0.07 (P value: 0.2, CeO_2 vs no NP control). The toxicity of CeO_2 NPs is found to be concentration dependent and this effect should be considered when implementing CeO_2 as a radioprotector.

Efficacy of CeO_2 NPs when used in synergy with different X-ray beams

The gliosarcoma cell line, 9L, was exposed to CeO_2 NPs at a concentration of 50 μg/ml during a 24 h incubation period prior to irradiation. The control flasks were incubated in the absence of the NP. All conditions remained constant besides the presence and absence of the NP. The first X-ray beam used was a 150 kVp beam and was chosen for both, its clinical relevance and to maximise the dose enhancement to the CeO_2 doped medium to a water equivalent medium based on the formalism described by Corde et al.[28] The 150 kVp beam produces an effective energy of 65 keV which lies close to, yet above the energy required to maximise dose enhancement (i.e.

54 keV). The cells were exposed to a range of doses up to 8 Gy. The samples were irradiated using either a 150 kVp or 10 MV X-ray beam to probe the effectiveness of CeO_2 NPs across a range of beam energies. Cell survival curves were produced using the clonogenic cell survival assay. This technique enabled any effect caused by the presence of the NP to be observed and quantified. The results show that the 9L cell line has a response that varies with treatment beam energy (Figure 3). The radiobiological parameters (α, β) for 9L cells are investigated for different radiation sources in the presence and absence of CeO_2 NPs. It is evident that CeO_2 NPs exhibit a protective effect to 9L cells when irradiated using a 10 MV photon beam (Figure 3, **A**). A higher surviving fraction at all doses was observed in the presence of CeO_2 NPs relative to the control sample. The radiosensitivity of 9L cells decreases in the presence of CeO_2 NPs with a corresponding increase in the damage repair as portrayed throughout table 1. A PER value of 1.23 ± 0.003 is achieved during the 10 MV treatment, confirming the radioprotective ability of CeO_2 NPs. A contrary effect is observed in response to exposure from the 150 kVp X-ray beam (Figure 3, **B**), where the surviving fraction in the presence of CeO_2 NPs is similar to the 9L control sample, revealing the consequence of the high-Z component of CeO_2 NPs. We observe a minor increase in radiosensitivity of 9L cells in the presence of CeO_2 coupled with the lack of evidence of damage repair, which is confirmed from the linear trend of the survival curve (Table 1). Subsequently, a PER close to unity is deduced, suggesting that CeO_2 NPs possess an energy-dependent radioprotection efficacy. We believe that a counterbalance between the sensitisation effect caused by increases in the RBE at lower photon energies[15,29] and the radioprotection offered through CeO_2's free-radical scavenging ability[6] is responsible for these energy-dependent effects.

Discussion

The application of CeO_2 NPs to clinical radiation protection is the subject of numerous studies and development[3,5–7]. Nanomedicine is a vastly expanding and alternative approach to existing medicines with applications ranging from diagnostic imaging and therapeutic radiation enhancement to radiation protection[6,15,30]. Minimising radiation-induced side effects is the focus of many studies and the catalyst in the production and development of novel approaches to radiation protection[28,31]. Scavenging free radicals is the most common approach used to provide

radiation protection. Development of new and improved radioprotectors as an alternative to amifostine is of great importance as a result of its clinical limitations[3,9].

We synthesised CeO_2 NPs using spray pyrolysis techniques for their application in radiation protection. High nanoparticle yield and reproducible characteristics such as size, phase and crystallinity are key advantages provided by our synthesising approach over alternative techniques of nanoparticle production[32]. Characterisation of our synthesised sample using XRD revealed important properties that were essential for our application. Results show that we have a nanoparticle sample with a single cubic phase, existing as CeO_2 upon comparison with the ICSD. The broad diffraction peaks (Figure 1) confirm the nano-crystallinity of CeO_2, with the mean crystallite size measured to range from 6–8 nm. Tarnuzzer et al.[7] report parallel findings with their XRD analysis of CeO_2, enabling us to suggest that our synthesised sample also exhibits these autoregenerative antioxidant effects for radiation protection. The HR-TEM image of CeO_2 shows crystallite sizes that correlate with that determined in our X-ray diffraction analysis. Distinct lattice fringes are observed, supporting the presence of a cubic structure with the distance between successive fringes deduced to be 3.15 Å, consistent with our diffraction data and the PDF card no. 01-089-8436 as published in the ICS database. Light micrographs of 9L cells incubated with CeO_2 NPs show that they are randomly distributed, i.e. around, on and alternately in the cells. However at such magnification, it is not possible to visualise intracellular localisation. Using flow cytometric analysis we deduce that CeO_2 NPs can be internalised in 9L cells. The internalisation is confirmed as a result of increases in the measured cell side scatter (data not shown), a technique utilised by Busch et al.[33] Results of the gas sorption analysis show a nanocrystalline surface area of 51 m^2/g, supporting the nanoscale crystallite size recorded. It is well known that the size of a nanoparticle is related its surface area, where smaller particles have greater surface areas[11]. Increasing the surface area could therefore act to maximise any related free-radical scavenging properties of CeO_2 NPs.

The toxicity of CeO_2 NPs to 9L cells was tested to elucidate its clonogenic survival at concentrations up to 500 μg/ml. We utilised mimetic experimental conditions to that used in radiation exposures, maximising the validity of the reported outcomes. Following a 24 h incubation of 9L cells with CeO_2 NPs, we report insignificant toxic effects at 50 μg/ml, consistent with other published literature[6,7,27]. Inconsistent conclusions have been made in regard to the toxic effects

of CeO_2 NPs, a factor requiring further development[26]. It is well documented that the size and structure of nanoparticles, influenced by the production process, dictate their toxicity[6,26]. Additional factors which should be investigated include: oxygen non-stoichiometry and balance of Ce3+/Ce4+ cation states, exposure time, concentration and aggregation of the nanoparticle, and also cell type as different toxic responses may occur[10].

It has been well established that CeO_2 NPs utilise a unique free-radical scavenging ability to provide radioprotection in both cell culture and murine models. Important factors influencing the effectiveness of CeO_2 include: cell sensitivity, NP concentration and synthesis and these factors should be further developed and understood in steps toward clinical acceptance.

Figure 3A clearly indicates that the CeO_2 NPs provide protection against radiation induced damage to gliosarcoma (9L) cells. Cell survival curves provide a wealth of information — not only a comparison of the response of cells exposed to radiation in the presence and absence of CeO_2, but the influence of CeO_2 on the radiobiological parameters, α and β used in the LQ model. Using a 10 MV photon beam, we record radioprotection at all doses up to 8 Gy with CeO_2 NPs at a concentration of 50 μg/ml. This radioprotection is supported by the increase in damage repair (β) and decrease in radiosensitivity (α) under the LQ model data interpretation observed in the presence of CeO_2 NPs. While statistically there is no significant difference between the two survival curves at 150 kVp, analysis of the data under the LQ model indicates an increased linearity of the survival curve in the presence of the NP. Investigation of the radiobiological parameters within the LQ model shows a small increase in the radiosensitivity when CeO_2 NPs are present. Within the LQ model the increased linearisation is interpreted as a change in the radiation spectrum. Therefore the increased linearity of the logarithmic cell survival suggests that CeO_2 NPs enable more direct damage effects to occur due to the additional enhancement in the field of low energy electrons.

The observed energy dependence of the PER efficacy (for 10 MV and 150 kVp) can be explained as a counterbalance between the free-radical scavenging ability of CeO_2 and the increased RBE due to lower energy radiations. The increase in the RBE is, in part, influenced by the macroscopic dose enhancement from the mass-energy absorption of CeO_2 and the increased yield of Auger electrons[29,34,35]. This energy dependence is also influenced by the increased production of photo-electrons, with a cross-section that is inversely proportional with energy (Figure 4). Photoelectric

interactions are important to consider for compounds such as CeO_2 as the effective atomic number (Z_{eff}=54)[36] has a strong influence on the photoelectric cross-section[13]. Photoelectric interactions stimulate two main processes – the ejection of characteristic X-rays and Auger electron cascades[37,38]. Auger electrons increase the average LET of the resultant secondary particles maximising the efficiency of these radiations through denser ionisations, imparting more direct damage which in turn reduces the abundance of reactive oxygen species responsible for indirect damage[17]. The 150 kVp X-rays yield a greater proportion of these higher LET particles than the 10 MV photon beam in the presence of CeO_2 NPs, supporting the energy dependent efficacy of radioprotection that we observe. Ideally, a radioprotective compound would have a low atomic number to minimise effects such as energy dependent protection. The use of low-Z radioprotectors is supported by the current "gold standard" clinical radioprotector, amifostine, which has a low effective atomic number (Z_{eff}=11). As radioprotectors generally function along a chemical pathway, the cross-section for the production of secondary particles should be minimised. The effect of the atomic number on the total photon interaction cross-section supports the notion that idealistic radioprotectors should have a low atomic number in order to be less dependent of the X-ray field energy spectra (Figure 4, **B**).

In conclusion we have demonstrated that the radioprotection (via free-radical scavenging) efficacy of the CeO_2 nanoparticle depends on the spectra of X-ray radiation. Our hypothesis is that the change in efficacy is driven by the high-Z component of CeO_2 that leads to a modification of the electron spectra in close proximity to the nanoparticles that can counterbalance the radioprotection efficacy of CeO_2. The electron spectra is modified through the increased production of low energy secondary electrons (including Auger cascades) that are generated due to predominance of the photoelectric effect at kilovoltage X-ray energies. The influence of these low energy electrons, with high LET, is reflected in the change of the shape of the survival curve for 9L cells exposed to CeO_2 nanoparticles and irradiated with 150 kVp X-rays compared to 10 MV X-rays, which adds weight to our hypothesis. Therefore we have highlighted a very interesting phenomenon that must be considered if radiation protection drugs for use in radiotherapy are developed based on the CeO_2 nanoparticle. This is particularly important in the case of cancer treatment delivered by different photon fields (e.g. superficial cancer treatment with 100 - 150 kVp photons in comparison with external beam radiotherapy delivered by 6-

18 MV photons) where we have shown that the changes in the free-radical scavenging efficacy of CeO_2 nanoparticles are pronounced. The scientific interest in the development of CeO_2 NPs as a radioprotecting agent is evident throughout the widespread literature that contains both, *in-vitro* and *in-vivo* models[3,5–8,10,24–27]. Expanding our knowledge in the application and functionality of CeO_2 NPs will continue with the long term goal of clinical implementation.

Acknowledgments

We gratefully acknowledge the Illawarra Health & Medical Research Institute for the use of the facility.

References

[1] Allard, E., Jarnet, D., Vessieres, A., Vinchon-Petit, S., Jaouen, G., Benoit, J., et al. Local delivery of ferrociphenol lipid nanocapsules followed by external radiotherapy as a synergistic treatment against intracranial 9L glioma xenograft. Pharm Res 2010;27:56–64.

[2] Metcalfe, P., Kron, T., Hoban, P.. The Physics of Radiotherapy, X-rays and Electrons. Madison, Wisconsin: Medical Physics Publishing; 2007.

[3] Madero-Visbal, R.A., Alvarado, B.E., Colon, J.F., Baker, C.H., Wason, M.S., Das, S., et al. Harnessing nanoparticles to improve toxicity after head and neck radiation. Nanomedicine 2012;xx:1–9. Doi:10.1016/j.nano.2011.12.011.

[4] Castedo, M., Perfettini, J., Roumier, T., Andreau, K., Medema, R., Kroemer, G.. Cell death by mitotic catastrophe: a molecular definition. Oncogene 20041;23:2825–2837.

[5] Rzigalinski, B.A., Bailey, D., Chow, W., Kuiry, S.C., Patil, S., Merchant, S.. Cerium oxide nanoparticles increase the lifespan of cultured brain cells and protect against free radical and mechanical trauma. FASEB J 2003;17:606–606.

[6] Colon, J., Herrera, L., Smith, J., Patil, S., Komanski, C., Kupelian, P., et al. Protection from radiation-induced pneumonitis using cerium oxide nanoparticles. Nanomedicine 2009;5:225–231.

[7] Tarnuzzer, R.W., Colon, J., Patil, S., Seal, S.. Vacancy engineered ceria nanostructures for protection from radiation-induced cellular damage. Nano Lett 2005;5:2573–2577.

[8] Rzigalinski, B.A., Meehan, K., Davis, R.M., Xu, Y., Miles, W.C., Cohen, C.A.. Radical nanomedicine. Nanomedicine 2006;1:399–412.

[9] Grdina, D., Murley, J., Kataoka, Y.. Radioprotectants: Current status and new directions. Oncology 2002;63:2–10.

[10] Lin, W., Huang, Y., Zhou, X., Ma, Y.. Toxicity of cerium oxide nanoparticles in human lung cancer cells. Int J Toxicol 2006;25:451–456.

[11] Sager, T.M., Porter, D.W., Robinson, V.A., Lindsley, W.G., Schwegler-Berry, D.E., Castranova, V.. Improved method to disperse nanoparticles for in vitro and in vivo investigation of toxicity. Nanotoxicology 2007;1:118–129.

[12] Buzea, C., Pacheco, I.I., Robbie, K.. Nanomaterials and nanoparticles: sources and toxicity. BioInterphases 2007;2:17–71.

[13] Attix, F.. Introduction to Radiological Physics and Radiation Dosimetry. Weinheim, Germany: Wiley-VCH; 2004.

[14] Rahman, W.N., Bishara, N., Ackerly, T., He, C.F., Jackson, P., Wong, C., et al. Enhancement of radiation effects by gold nanoparticles for superficial radiation therapy. nanomedicine 2009;5:136–142.

[15] Butterworth, K.T., Coulter, J.A., Jain, S., Forker, J., McMahon, S.J., Schettino, G., et al. Evaluation of cytotoxicity and radiation enhancement using 1.9 nm gold particles: potential application for cancer therapy. Nanotechnology 2010;21:295101–295709.

[16] Kahn, F.M.. The Physics of Radiation Therapy. Maryland, USA: Williams and Wilkins; 1994.

[17] Tubiana, M., Dutreix, J., Wambersie, A.. Introduction to Radiobiology. United Kingdom: Taylor & Francis; 1990.

[18] Sastry, K.S.R.. Biological effects of the Auger emitter iodine-125 A review. Report No. 1 of AAPM Nuclear Medicine Task Group No. 6. Medical Physics 1992;19:1361–1370.

[19] Konstantinov, K., Stambolova, I., Peshev, P., Darriet, B., Vassilev, S.. Preparation of ceria films by spray pyrolysis method. Int J Inorg Mater 2000;2:277–280.

[20] Truffault, L., Winton, B., Choquenet, B., Andreazza, C., Simmonard, C., Devers, T., et al. Cerium oxide based particles as possible alternative to ZnO in sunscreens: Effect of the synthesis method on the photoprotection results. Mater Lett 2012;68:357–360.

[21] Langdon, S.. Cancer Cell Culture: methods and protocols. Totowa, New Jersey: Humana Press; 2004.

[22] Puck, T.T., Marcus, P.I.. Action of x-rays on mammalian cells. J Exp Med 1956;103:653–666.

[23] Brenner, D.. The Linear-Quadratic model is an appropriate methodology for determining isoeffective doses at large doses per fraction. Semin Radiat Oncol 2008;18:234–239.

[24] Thill, A., Zeyons, O., Spalla, O., Chauvat, F., Rose, J., Auffan, M., et al. Cytotoxicity of CeO_2 nanoparticles for escherichia coli. physico-chemical insight of the cytotoxicity mechanism. Environmental Science and Technology 2006;40:6151–6156.

[25] Nalabotu, S.K., Kolli, M.B., Triest, W.E., Ma, J.Y., Manne, N.D., Katta, A., et al. Intratracheal instillation of cerium oxide nanoparticles induces hepatic toxicity in make Sprague-Dawley rats. Int J Nanomed 2011;6:2327–2335.

[26] Park, E., Choi, J., Park, Y.. Oxidative stress induced by cerium oxide nanoparticles in cultured BEAS-2B cells. Toxicology 2008;245:90–100.

[27] Xia, T., Kovochich, M., Liong, M., Madler, L., Gilbert, B., Shi, H., et al. Comparison of the mechanism of toxicity of zinc oxide and cerium oxide nanoparticles based on dissolution and oxidative stress properties. ACS Nano 2008;2:2121–2134.

[28] Corde, S., Joubert, A., Adam, J.F., Charvet, A.M., Le Bas, J.F., Esteve, F., et al. Synchrotron radiation-based experimental determination of the optimal energy for

cell radiotoxicity enhancement following photoelectric effect on stable iodinated compounds. British Journal of Cancer 2004;91:544–551.

[29] McMahon, S.J., Hyland, W.B., Muir, M.F., Coulter, J.A., Jain, S., Butterworth, K.T., et al. Biological consequences of nanoscale energy deposition near irradiated heavy atom nanoparticles. Sci Rep 2011;1:1–9.

[30] Moghimi, S.M., Hunter, A.C., Murray, J.. Nanomedicine: current status and future prospects. FASEB J 2005;19:311–330.

[31] Hendry, J.H., Jeremic, B., Zubizarreta, E.. Normal tissue complications after radiation therapy. Pan Am J Public Health 2006;20:151–160.

[32] Madler, L., Kammler, H.K., Mueller, R., Pratsinis, S.. Controlled synthesis of nanostructured particles by flame spray pyrolysis. J Aerosol Sci 2002;33:369–389.

[33] Busch, W., Bastian, S., Trahorsch, U., Iwe, M., Kuhnel, D., MeiBner, T., et al. Internalisation of engineered nanoparticles into mammalian cells in-vitro: influence of cell type and particle properties. J Nanopart Res 2011;13:293–310.

[34] Robar, J.L., Riccio, S.A., Martin, M.A.. Tumour dose enhancement using modified megavoltage photon beams and contrast media. Phys Med Bio 2002;47:2433–2449.

[35] McMahon, S.J., Mendenhall, M.H., Jain, S., Currell, F.. Radiotherapy in the presence of contrast agents: a general figure of merit and its application to gold nanoparticles. Phys Med Bio 2008;53:5635–5651.

[36] Boone, J.M., Chavez, A.. Comparison of X-ray cross sections for diagnostic and therapeutic medical physics. J Med Phys 1996;23:1997–2005.

[37] Kobayashi, K., Usami, N., Porcel, E., Lacombe, S., Le Sech, C.. Enhancement of radiation effect by heavy elements. Mutat Res 2010;704:123–131.

[38] Porcel, E., Liehn, S., Remita, H., Usami, N., Kobayashi, K., Furusawa, Y., et al. Platinum nanoparticles: a promising material for future cancer therapy? Nanotechnology 2010;21:1–7.

Figure 1: X-ray diffraction spectrum of the CeO_2 NP sample synthesised by spray pyrolysis **(A)**. Data was acquired using an automated GBC® eMMA X-ray Diffractometer. X-ray diffraction peaks were assigned Miller indicies in correlation with the ICSD. High Resolution Transmission Electron Microscopy image of CeO_2 NPs synthesised using spray pyrolysis techniques **(B)**.

Figure 2: The surviving fraction of 9L cells exposed to CeO_2 NPs during a 24 h exposure at increasing concentrations up to 500 μg/ml. The toxicity was measured using the clonogenic cell survival assay. Surviving fraction data is presented with uncertainties given as one standard deviation with statistical significance measured with a P value ≤ 0.05.

Figure 3: 9L clonogenic cell survival after irradiation with 10 MV **(A)** or 150 kVp **(B)** X-ray beams in the presence (triangle) and absence (square) of CeO_2 NPs at a concentration of 50 μg/ml. All uncertainties are presented with one standard deviation made from duplicate samples which are measured in triplicate.

Figure 4: Energy dependence of the mass-energy absorption coefficients for the three main radiation interactions are highlighted as a function of treatment beam energy for CeO_2 (**A**). The total mass-energy absorption coefficients for amifostine and CeO_2 are shown over a range of energies (**B**) highlighting the influence on the mass-energy absorption coefficient through increases in atomic number.

Table 1: Summary of the radiobiological parameters for 9L cells exposed to different radiation sources in the presence and absence of CeO_2 NPs. The LQ model was used to fit the surviving fraction data in KaleidaGraph, extracting the α and β constants. All uncertainties listed are given as one standard deviation.

Table 1

Click here to download Table: Table 1.docx

Experimental Parameters				
	Control		50 µg/ml	
Radiation source	α (Gy^{-1})	β (Gy^{-2})	α (Gy^{-1})	β (Gy^{-2})
150 kVp X-rays	0.21 ± 0.03	0.009 ± 0.004	0.30 ± 0.04	--
10 MV X-rays	0.20 ± 0.06	0.013 ± 0.008	0.06 ± 0.04	0.019 ± 0.005

Revised Figure 1

Click here to download Figure: Figure1.eps

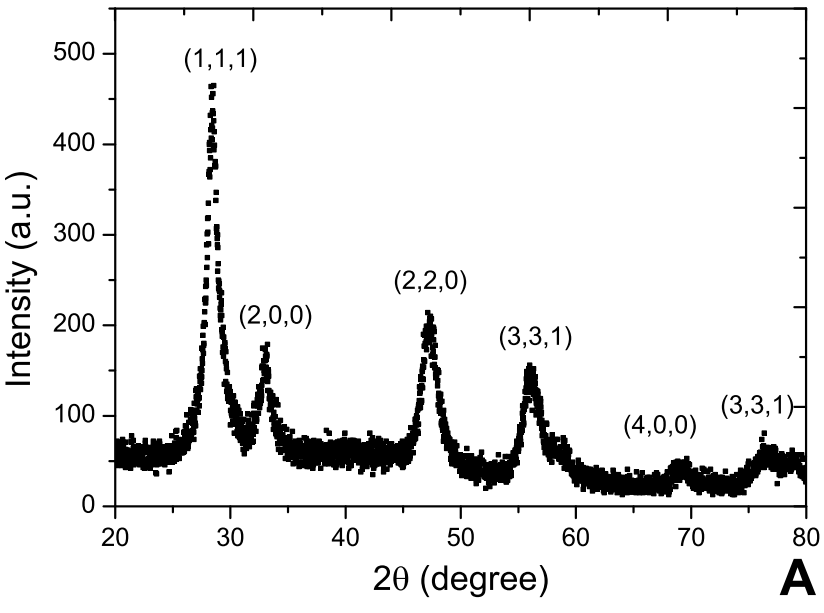

A

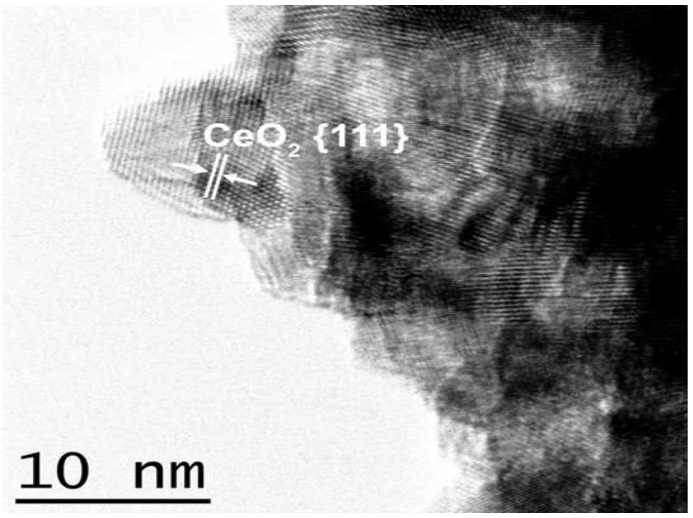

B

Revised Figure 2

Click here to download Figure: Figure2.eps

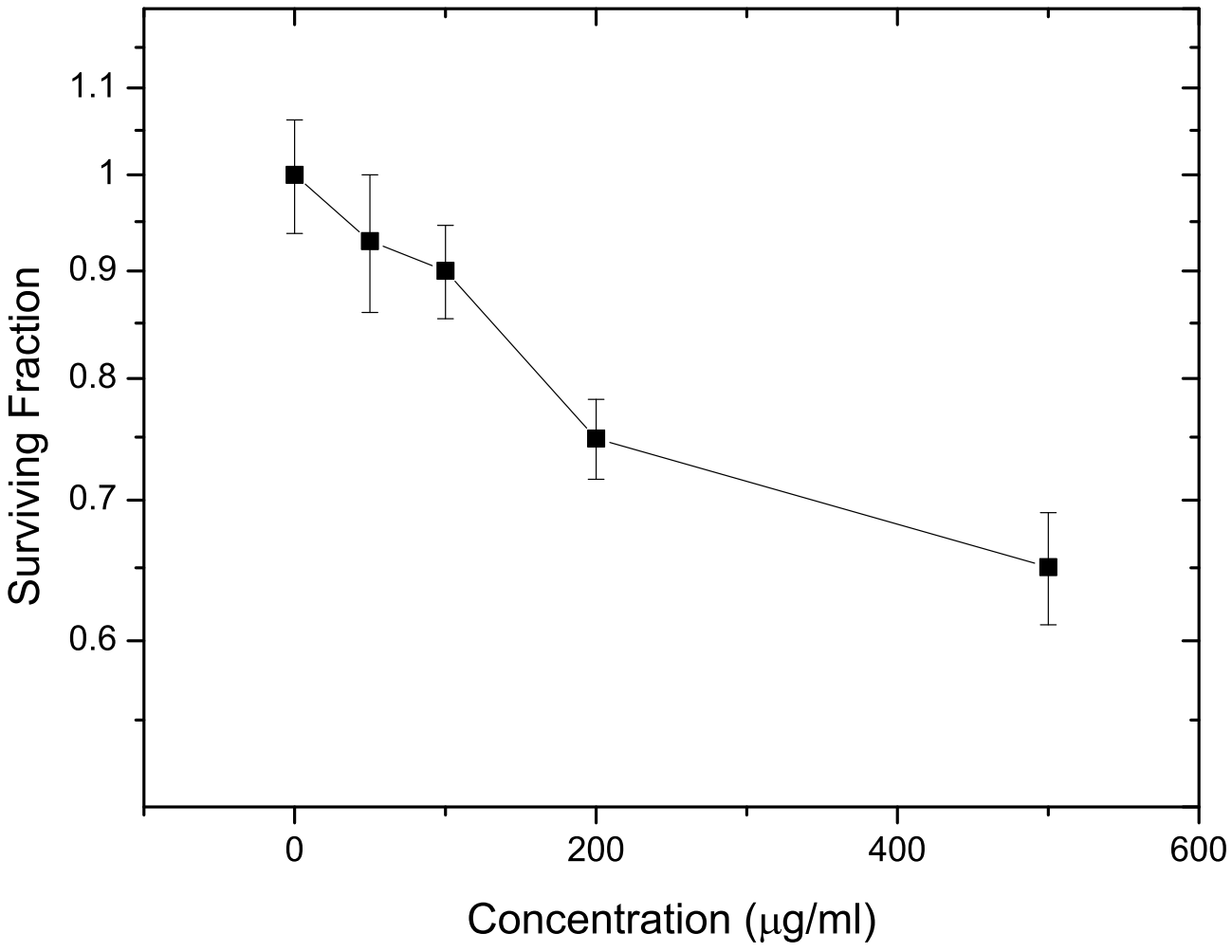

Revised Figure 3

Click here to download Figure: Figure3.eps

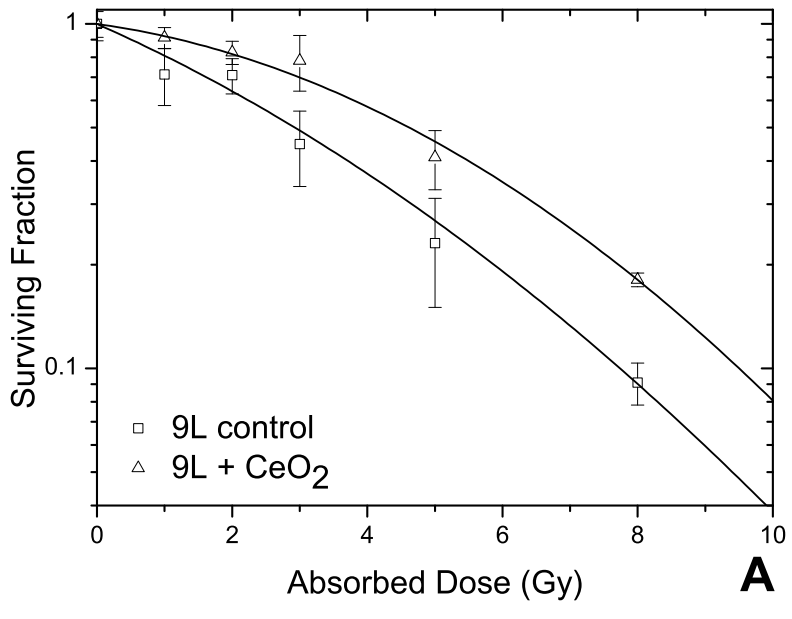

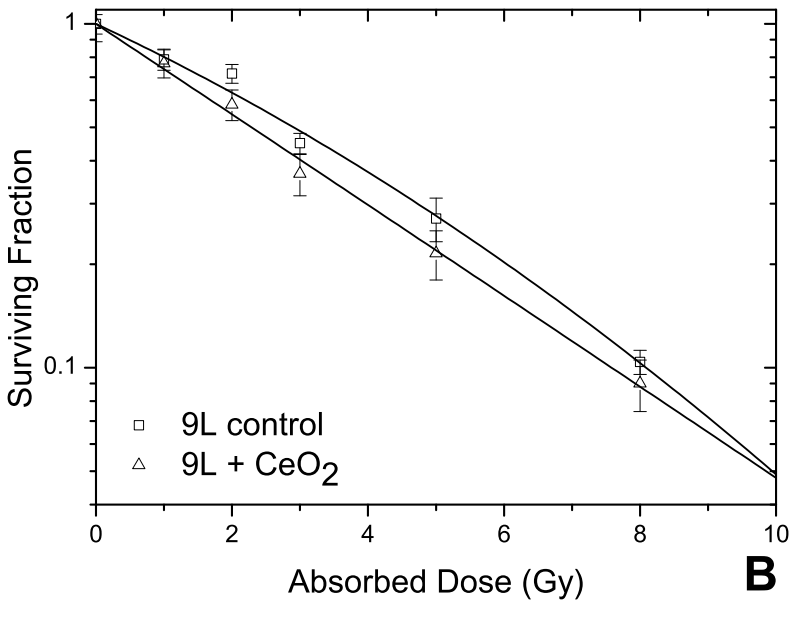

Revised Figure 4

Click here to download Figure: Figure4.eps